Influence of Succinite Additives on the Crystal Structure and Orientation of Composite PA6 Nanofibers

Inga Lasenko
JLU Technologies Ltd
(of Affiliation)
Riga, Latvia
info@jlutechnologies.com

Abstract. **Give this article delves into the investigation of the crystal structure and crystalline orientation of composite polyamide 6 (PA6) nanofibers. The study aims to elucidate the impact of crystallinity and crystalline orientation on the properties of composite nanofibers, which were manufactured by the electrospinning process of Nylon 6/formic acid (HCOOH) polymer solutions at concentrations of 16%, 20% and 28%, incorporating 0.25% succinite powder with particle sizes ranging from 5 to 20 nm. The average diameters of the resulting nanofiber mats were systematically measured, revealing dimensions of 50±15 nm, 90±18 nm, and 340±78 nm, respectively. Using wide-angle X-ray diffraction (WAXD) analysis, the study provides a detailed examination of how the concentration of PA6 and the inclusion of organic succinite additives influence the crystal structure and crystalline orientation within the polymer matrix. In particular, it highlights the effects observed at smaller diameters of composite nanofibers, where enhanced macromolecular alignment is coupled with reduced crystallinity, marking the first comprehensive exploration of these phenomena in individual composite nanofibers. Research demonstrates that the relative distribution of different crystalline phases varies among samples with different average diameters. Notably, the sample with the smallest average diameter of 50 nm showcased a singular crystalline peak at $2\theta=21.23°$, closely aligning with the theoretically reported value for the γ phase ($2\theta=21.4°$). On the contrary, samples with larger average diameters revealed progressively more distinct shoulders on X-ray diffraction patterns, indicative of the α phase. A notable increase of approximately 25% was observed as the diameter of the composite nanofibers decreased. Furthermore, the composite nanofibers of smaller diameter presented a narrower full width at Half Maximum (FWHM), suggesting enhanced orientation for both observed phases. This study not only contributes to understanding of the influence of nanofiber composition and structure on their physical properties but also opens new avenues for the tailored design of nanofiber based composites for advanced engineering applications.**

I. INTRODUCTION

This it is known that studies of the structural parameters (crystal structure and crystalline orientation) of the polymers allow to attribute their mechanical behavior (increased strength, modulus, and toughness) at small nanofiber diameter to improved macromolecular alignment coupled with low crystallinity [1], [2]. This combination of structural features of polymers is unusual and almost impossible to achieve in traditional manufacturing techniques. It is important to understand whether such behavior is universal in electrospinning or is dependent on the polymer/solvent system. The structural features of the polymers likely depends on the crystal structure and crystalline orientation of the polymer system, especially important if it is a composite structure (where different polymers may be included) [3], [4]. In order to examine the universality of these features and their impact on the mechanical properties, a polymer system that is more crystallizable.

To date, some attempts have been made to systematically study the influence of polymer structural parameters (crystalline structure and crystalline orientation) on nanofibers with a wide range of diameters [5]–[8], obtained as a function of varying polymer concentration [9]–[11].

For this structural analysis, PA6 was chosen. It is one of the most widely used engineering plastics due to outstanding mechanical properties such as high tensile strength. In addition, Nylon 6 fibres also exhibit high toughness, good wear, chemical resistance, and easy processing [6], [8], [12]. It was considered an ideal replacement of metal and rubber used in the fibre industry to meet enormous market requirements from military to civilian applications [7]. Nylon 6 is an easily crystallizeable polymer and offers a good test case for comparison with other polymer materials.

It is known that nylon, a man-made semi-crystalline polymer, is one of the three major polymers used in industry. Nylon can have a different ratio of mixtures of diamines ($-NH_2$) and diacids ($-COOH$) in repeated units, offering many possible tailoring for specific use. The polarity of the amide group of Nylon results in strong hydrogen bonds within the material.

The different ratio of the mixture of the two groups results in a different structure of the polymer and thus leads to different properties. Besides this, the backbone of the nylon polymer chain is symmetrically aligned, and as a result, it easily facilitates the crystalline structure that is useful for the formation of fibres. So, Nylon 6 is known to be easily produced in the form of fibre through conventional spinning and electrospinning. Nylon 6 is one type of chemical structure, where one member of the nylon consisted of six carbons in the repeated unit called Nylon 6 (or poly-(ε-caproamide)) and emerged as a new family of Nylon 6.

The organic polymer (succinite powder) was chosen as an additive, which could potentially be used as part of the polymer structure to provide ultraviolet protection (based on our previous studies). As is known, any mixing of polymers with different hardness, and, accordingly, density, is decisive importance on the mechanical properties of the resulting polymer structures (in this case is the nano fibers).

Thus, based on studies of the structural parameters of the polymer Nylon 6 (crystal structure and crystalline orientation, where combination of structural features of polymer almost impossible to achieve in traditional manufacturing techniques) follow the main task of the work - that is to study the influence of succinite additives on the crystal structure and orientation of composite PA6 nanofibers with three range of diameters obtained as a function of varying polymer concentration.

II. Material and Methods

To observe the influence of Nylon 6 polymer structural parameters (crystal structure and crystalline orientation) on nanofibers with three range of diameters obtained as a function of varying polymer concentration, several structural investigations were conducted. To examine the crystal structure, random mats were electrospun from 16%, 20%, and 28% Nylon 6/HCOOH polymer solutions. The average diameter was obtained for each of the mats (50±15 nm, 90±18 nm, and 340±78 nm, respectively).

Nylon 6 (PA-6) pellets (MW = 10,000, purchased from Sigma-Aldrich, Germany) and 0.25 wt/wt succinite (Baltic amber) powder (JLU Technologies Ltd, Latvia; CAS: 9000-02-6; EC: 232-520-0; 5-20 nm, d98%<20 nm) were mixed with Formic acid solution (98%, purchased from Sigma-Aldrich, Germany) to prepare 16-30 wt% solution, prepared on a hot plate for 12 hours (room temperature 22±1 °C; moisture content 60%). The diameters of the Nylon 6 composite nanofibers were controlled by electrospinning parameters such as voltage, needle gauge, and polymer solution concentration. Nylon 6 composite nanofibers were electrospun (Fisherbrand™ Single Syringe Pump, a needle-based electrospinning machine, USA) using 16.5 kV spinneret voltage from a 20 cm distance, 0.6-1 ml/h feed rate, and 22–27 gauge needle. The PA6 composite nanofibers were collected in a rotation dram collector (Shenzhen Tongli Tech Co Ltd, (D-608) Shenzhen, China; Rotating Collector RC-5000, D140, L50). The rotating speed of the drum collector was constant at 1800 rpm and aluminium foil (width 10 cm and coating thickness 35 μm; Vireo.de Merseburg, 06217, Germany) was used on the drum to collect composite nanofibers.

The morphology of Nylon 6 composite nano mats and diameter distribution for each polymer concentration (16 wt% 20 wt%, and 28 wt%) was obtained by capture SEM photographs, Hitachi's TM300 tabletop microscope SEM with a magnification of 1500, a vacuum of 10^{-2} Torr, an ion coating with six mA, a gold (Au) cover, and a coating thickness of 150 were used. Composite nanofiber diameter was acquired using the OrientationJ plug-in for the ImageJ programme (ImageJ, National Institutes of Health, Bethesda, MD, USA). The contrast of the SEM images was enhanced to observe the results. The determination of the mean diameter of the nanofiber and standard deviation was made possible by measuring the diameter of 100 nanofibers randomly selected from three SEM images.

Composite nanofiber mats were examined by wide angle X-ray diffraction (WAXD), using 1D wide angle Diffractormeter Ragaku with Cu Kα radiation, for the 2θ range from 5 to 50°.

In this study, a protocol [13] was used to examine the crystal orientation of PA 6 nanofiber. Electrospun Nylon 6 nanofiber bundles with average diameters of 90±18 nm and 340±78 nm were used. The respective morphology of the nanofibers is shown in Fig. 6 (a; d). The diameter distribution and degree of misalignment were measured based on SEM images, using Image J software. The degree of misalignment of the nanofibers from their respective main bundle axis for the two bundles were 90°±9° (D=90±18 nm) and 87°±7° (D=340±78 nm), respectively. The examination of the crystal orientation along the fiber direction was conducted using XRD transmission mode.

WAXD experiments of the composite nanofibers (composite nanofibers D=90±18 nm; D=340±78 nm) were performed by a BL03XU beamline with a wavelength of λ = 1.0 Å at SPring-8, Harima, Japan. The sample-to-detector distance for the measurements was set to 77 mm. Two-dimensional WAXD patterns were recorded with an exposure time of 1 s using a silicon-on-insulator photon imaging array sensor (SOPHIAS) as a detector. The lattice spacing and crystal lattice parameters were calculated by following the Wulff-Bragg condition from the obtained WAXD profile. The crystallinity of composite nanofibers (Xc) was determined through profile after the total pattern from WAXD was divided into crystalline and amorphous portions [14].

III. Results and Discussion

A. Crystal structure

If Nylon 6 has two main phases (α and γ). It is generally agreed that the α phase is an extended planar zigzag configuration, and it is thermodynamically stable. The γ phase is a pleated helical chain and is metastable. The parameters of the unit cell of two crystalline phases are as follows: α-crystalline phase (monoclinic cell, a = 0.956 nm, b = 1.724 nm (fibre axis), c = 0.801 nm, and β = 67.5°), and γ -crystalline phase (monoclinic cell, a = 0.933 nm b =

1.688 nm, c = 0.478 nm, and β = 121°) [15]. Fig. 1 demonstrates the molecular confirmation of these phases.

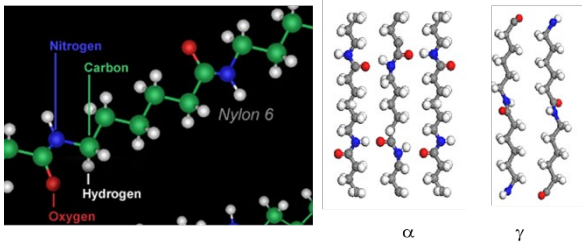Fig. 1. The conformation of α and γ phase crystal structure of Nylon 6 [16].

In addition to α and γ phases, there are several intermediate phases. They appear when an unstable γ phase transitions into a stable α phase. Fig. 2 (a-b) shows the theoretical WAXD patterns for the two main phases.
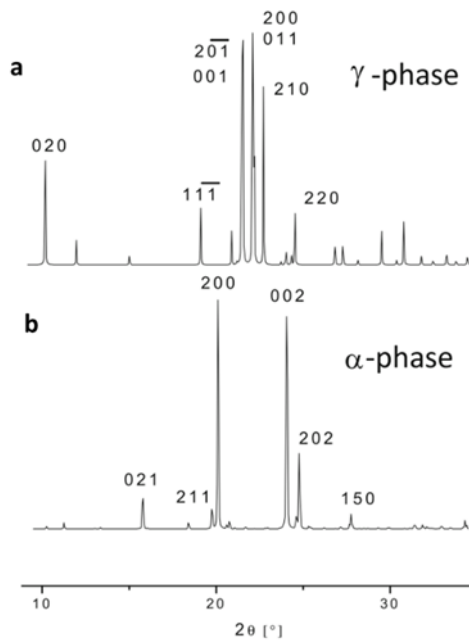

Fig. 2. The perfect theoretical crystal structures of two main crystal phases of the Nylon 6: a) the phase γ; b) the phase α [19].
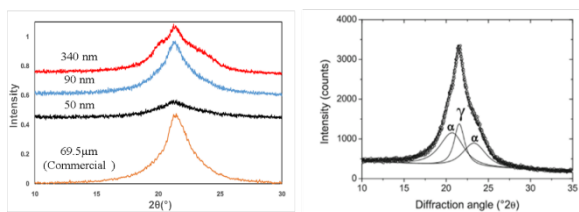

Fig. 3. XRD pattern of composite Nylon 6 fibres: a) experimental results of composite Nylon 6 nanofibers (size of average diameters 50±15 nm; 90±18 nm; 340±78 nm) with comparison of commercial microfiber: pure Nylon 6 (size of diameter 69.5±8 mkm); b) conventional spun nanofiber [17]. The diffraction lines of the individual phases (solid lines) obtained by fitting the measured intensities by three Pearson VII functions [19] and are labelled by diffraction indices. Only the line profiles corresponding to the spectral line Cu Kα are shown

As can be seen in the left panel of Fig. 3, the electrospun composite nanofibers exhibited a generally poor structure with wide overlapping peaks. Similarly to commercial fibre, this pattern corresponds to a mix of the α and γ

phases. The observed XRD pattern for electrospun nylon NFs is similar to patterns obtained from electrospun Nylon 6 nanofiber mats in the literature [9], [17]. The patterns in the literature [9], [18]are especially similar to our pattern for a mat with an average diameter of 340 nm.

The dominant feature in the XRD pattern is the peak that corresponds to the γ phase. Peaks corresponding to the α phase appear as shoulders in the pattern. It is reported that there are usually two characteristic peaks of the α-phase located at 2θ=20° and 23.7° in the XRD diffraction pattern of Nylon 6, corresponding respectively to (200) and (002)/(202) crystal planes [20]. The γ phase reflected peaks at around 2θ=10.7° and 21.4° corresponding to (020) and (001) crystal planes [21]–[23]. Zhudi Zhao and his coauthor studied crystalline and amorphous phases of the quenched Nylon 6 film and found a broad amorphous halo located at 2θ=21° [24]. It is clear that the relative mix of the different phases changed between samples with different average diameters.

The sample with an average diameter of 50 nm exhibited only one crystalline peak located at 2θ =21.23°, close to theoretical reported value for the γ phase (2θ= 21.4°) [17]. The samples with larger average diameters exhibited progressively more pronounced shoulders corresponding to the α phase.

The different crystal and amorphous peaks were deconvoluted using spacing diameters from the literature. Crystallinity was extracted from the XRD patterns after deconvolution, using a protocol similar to reference [25] (an example in Fig. 4 a-b). Crystallinity as a function of the average diameter of the composite nanofiber diameter (50±15 nm; 90±18 nm; 340±78 nm) is shown in Fig. 4-c.

The ~ 25% increase in composite polymer crystallinity was observed with the decrease in composite nanofiber diameter.
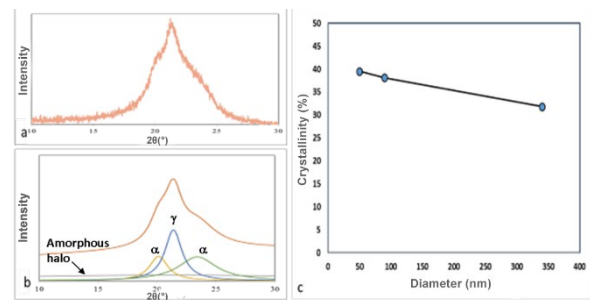

Fig. 4. The conformation of α and γ phase crystal structure of Nylon 6 [17]. a) XRD pattern of composite nanofiber with average diameter of 340±78 nm; b) peak fit of (a); (c) crystallinity of electrospun composite Nylon 6 nanofibers with three different diameters.

This result is consistent with DSC experiments carried out by collaborators at the University of Rouen Normandie, CNRS, and Groupe de Physique des Materiaux, France (Fig. 5) and can explain the slight decrease in strain-to-failure for thinner nanofibers. For example, compared with other mostly used polyacrylonitrile (PAN), behavior of PA 6 is different from that of PAN [26], where decrease in crystallinity was observed for smaller diameters.
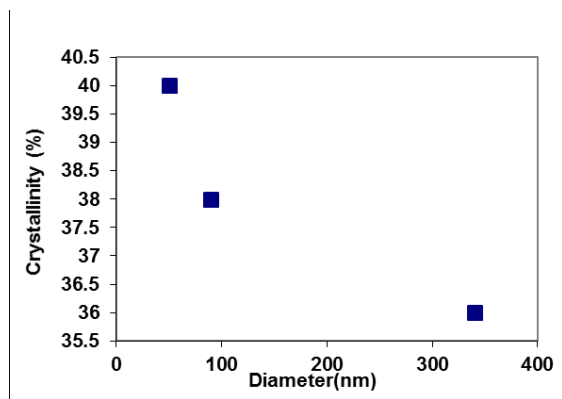
Fig. 5. Crystallinity as a function of composite nanofiber diameters (provided by University of Rouen Normandie, CNRS, and Groupe de Physique des Materiaux, France).

In electrospinning, fast solvent evaporation plays a role similar to fast quenching in traditional polymer manufacturing from melts. This fast process promotes nucleation of phases that are not in thermodynamic equilibrium (such as γ phase in Nylon 6) and is likely to be faster in thinner nanofibers. This can explain why larger diameter nanofibers exhibit a larger amount of the α phase. The differences in the size-dependent crystallinity behaviour between, for example, with PAN [27], and Nylon 6 nanofibers can be explained by the different crystallinities of these two polymer systems. The observed structural differences are also consistent with the differences observed in nanofiber strain-to-failure.

In addition, the electrospun Nylon 6 composite nanofibers showed a lower crystallinity than the conventional Nylon 6 microfibers [28]. This supports the hypothesis that even in a crystallisable polymer such as Nylon 6, the rapid solvent evaporation holds back the crystallisation process.

The crystal sizes for the different phases were extracted from the XRD patterns, using the Scherrer' equation (similar to Protocol [29]), shown in Table 1. The results showed that the crystal size of the crystal phases did not change significantly and remained well below nanofiber diameter. This indicates that crystal size did not play a significant role in the determination of mechanical properties.

TABLE 1 CRYSTAL SIZE OF EACH CRYSTAL PHASE FOR WELL-ALIGNED COMPOSITE NANOFIBERS WITH AVERAGE DIAMETERS OF 50, 90 AND 340 NM.

Nm	Coherence length (nm)	Nanofiber # 1 (D = 50±15 nm)	Nanofiber # 2 (D = 90±18 nm)	Nanofiber # 3 (D = 340±78 nm)
1	α_1	2.97	4.04	4.29
2	γ	4.23	4.03	4.62
3	α_2	3.93	3.84	2.07

B. Crystal orientation

Define WAXD experiments of composite PA6 nanofibers (composite nanofibers D=90±18 nm; D=340±78 nm) were performed (a similar protocol for crystal orientation research shown in [30]).

Electrospun composite Nylon 6 nanofiber bundles with average diameters of 90 and 340 nm were produced. The respective morphology of the composite Nylon 6 nanofibers was as shown in Fig. 6 a-d. The diameter distribution and the degree of misalignment were measured based on SEM images, using ImageJ software [31]. Homogeneous composite nanofibers with uniformly distributed succinite particles are observed. The degree of misalignment of the nanofibers from their respective main bundle axis for the two bundles was ±9° and ±7°, respectively (see the distribution of the orientation of the composite nanofibers in Fig. 6 b-e). The examination of the crystal orientation along the direction of the composite nanofiber was conducted using XRD transmission mode. WAXD 2D (two-dimensional) patterns of two bundles are shown in Fig. 6 (c-f).
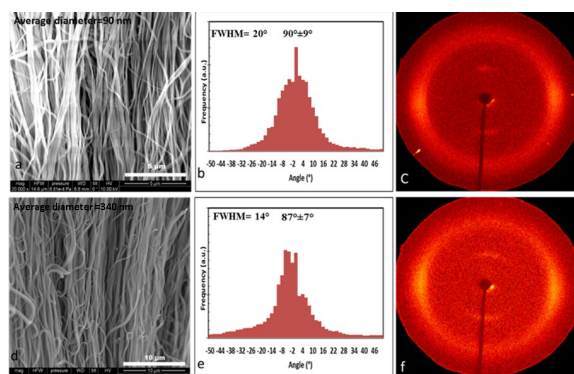

Fig. 6. The Comparison of the orientation of Nylon 6 nanofibers: a) morphology of aligned nanofiber bundles with average diameter of 90 nm; d) morphology of aligned nanofibers bundles with an average diameter of 340 nm; b) nanofibers orientation D=90±18 nm: along nanofiber direction; e) nanofibers orientation D=340±78 nm: of along nanofiber direction; c) WAXD 2D patterns of composite nanofiber D=90±18 nm; f) WAXD 2D patterns of composite nanofiber D=340±78 nm.

The extent of the double arcs in the diffraction pattern was used as an indicator of crystal orientation. The 2D pattern was converted into an azimuthal intensity scan, corresponding to the arcs from different crystal phases (Fig. 7 b-d; Fig. 8 b-d).
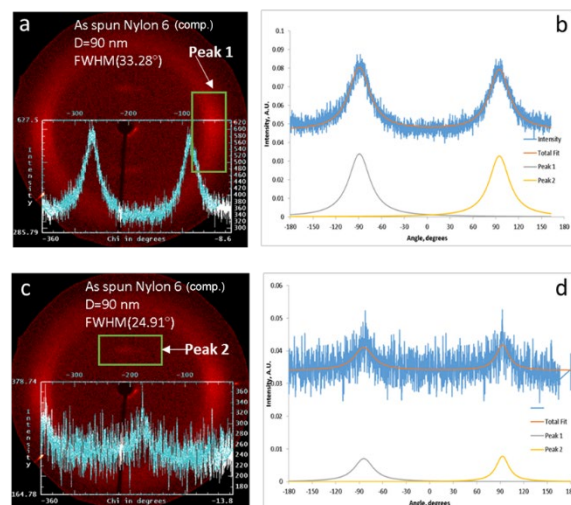

Fig. 7. The Crystal orientation in well-aligned composite nanofibers with diameter of 90±18 nm; a-c: WAXD patterns exhibited two main peaks: peak 1 (FWHM 33.28°) and peak 2 (FWHM 24.91°); b-d: 2 D pattern converted into an azimuthal intensity scan, corresponding to arcs from different crystal phases.

The WAXD patterns exhibited two main peaks. Peak 1 and peak 2 were labelled in Fig's: 7 (a-c) and 8 (a-c). Peak 1 corresponded to the γ phase, while peak 2 corresponded to a mixture of γ and α phases ((001) plane in the γ phase and (200) and (002)/(202) planes in the α phase). Peak 1 indicated that the crystalline plane (020) was parallel to the fibre direction. Peak 2 indicated that the mixture of crystal planes was perpendicular to the fibre axis. Full width at Half Maximum (FWHM) of the peaks in the azimuthal scan was used as an indicator of crystal orientation. Table 2 summarises the orientation parameters for the different phases.

TABLE 2 CRYSTAL ORIENTATION PARAMETERS OF ALIGNED COMPOSITE NANOFIBERS WITH AN AVERAGE DIAMETER OF 90 AND 340 NM.

Nm	Average Diameter (nm)	FWHM (°) - Mixture of α and γ phase	FWHM (°) - γ phase
1	90	33.3	24.9
2	340	37.9	50

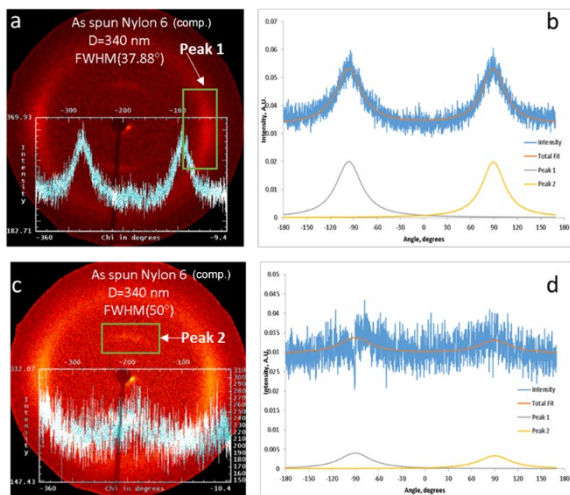Fig. 8. The Crystal orientation in well-aligned composite nanofibers with an average diameter of 340±78 nm; a c: the WAXD patterns exhibited two main peaks: peak 1 (FWHM 37.88°) and peak 2 (FWHM 50°); b-d: the 2 D pattern converted into an azimuthal intensity scan, corresponding to the arcs from different crystal phases.

Composite nanofibers with smaller diameters exhibited narrower full width at Half Maximum (FWHM) indicating better orientation, for both phases. Higher crystallinity and better crystal alignment in thinner nanofibers can explain the improvements in strength and modulus for these nanofibers.

This study not only contributes to understanding of the influence of nanofiber composition and structure on their physical properties but also opens new avenues for the tailored design of nanofiber based composites for advanced engineering applications [32]–[41], included an innovative recycled technologies of these materials [42]–[44]; because the modern industrial development has a high demand for new materials – with unique properties, combinations, and functionality [45]–[51].

IV. CONCLUSION

A study of the influence of the Nylon 6 structural characteristics of the composite polymer structure showed that the average diameter of the nanofiber depends on the concentration of the polymer in combination with 0.25% succinite, namely at a concentration of 16% the average diameter of the nanofiber is 50 nm; at 20% - 90 nm; at 28% - 340 nm. This is consistent with the reference literature, where a similar pattern (as the polymer concentration decreases, the average nanofiber diameter during electrospinning increases) was observed for pure polymer compositions (for example, PA6; PAN).

It was shown that the relative mix of the different phases changed between samples with different average diameters. The sample with an average diameter of 50 nm exhibited only one crystalline peak located at 2θ=21.23°, close to theoretical reported value for the γ phase (2θ=21.4°). The samples with larger average diameters exhibited progressively more pronounced shoulders corresponding to the α phase. The ~ 25% increase in composite polymer crystallinity was observed with the decrease in composite nanofiber diameter.

Electrospun Nylon 6 composite nanofibers showed a lower crystallinity than conventional Nylon 6 fibres. This supports the hypothesis that even in a crystallisable polymer such as Nylon 6, the rapid solvent evaporation holds back the crystallisation process.

Composite nanofibers with smaller diameter exhibited a narrower full width at Half Maximum (FWHM) indicating better orientation for both phases. Higher crystallinity and better crystal alignment in thinner nanofibers can explain the improvements in strength and modulus for these nanofibers.

REFERENCES

[1] M. Naraghi, S. N. Arshad, and I. Chasiotis, "Molecular orientation and mechanical property size effects in electrospun polyacrylonitrile nanofibers," *Polymer (Guildf).*, vol. 52, no. 7, pp. 1612–1618, 2011, doi: 10.1016/j.polymer.2011.02.013.

[2] D. Tian, C. H. He, and J. H. He, "Macromolecule orientation in nanofibers," *Nanomaterials*, vol. 8, no. 11, 2018, doi: 10.3390/nano8110918.

[3] L. S. Loo and K. K. Gleason, "Insights into structure and mechanical behavior of α and γ crystal forms of nylon-6 at low strain by infrared studies," *Macromolecules*, vol. 36, no. 16, pp. 6114–6126, 2003, doi: 10.1021/ma034213v.

[4] H. S. SalehHudin, E. N. Mohamad, W. N. L. Mahadi, and A. Muhammad Afifi, "Multiple-jet electrospinning methods for nanofiber processing: A review," *Mater. Manuf. Process.*, vol. 33, no. 5, pp. 479–498, 2018, doi: 10.1080/10426914.2017.1388523.

[5] M. B. Bazbouz and G. K. Stylios, "The tensile properties of electrospun nylon 6 single nanofibers," *J. Polym. Sci. Part B Polym. Phys.*, vol. 48, no. 15, pp. 1719–1731, 2010, doi: 10.1002/polb.21993.

[6] K. Y. Hwang, S. D. Kim, Y. W. Kim, and W. R. Yu, "Mechanical characterization of nanofibers using a nanomanipulator and atomic force microscope cantilever in a scanning electron microscope," *Polym. Test.*, vol. 29, no. 3, pp. 375–380, 2010, doi: 10.1016/j.polymertesting.2010.01.002.

[7] H. Mahfuz *et al.*, "Enhancement of strength and stiffness of Nylon 6 filaments through carbon nanotubes reinforcement," *Appl. Phys. Lett.*, vol. 88, no. 8, 2006, doi: 10.1063/1.2179132.

[8] L. Li, L. M. Bellan, H. G. Craighead, and M. W. Frey, "Formation and properties of nylon-6 and nylon-6/montmorillonite composite nanofibers," *Polymer (Guildf).*, vol. 47, no. 17, pp. 6208–6217, 2006, doi: 10.1016/j.polymer.2006.06.049.

[9] N. Kimura, B. S. Kim, and I. S. Kim, "Effects of Fe2+ ions on morphologies, microstructures and mechanical properties of electrospun nylon-6 nanofibers," *Polym. Int.*, vol. 63, no. 2, pp. 266–272, 2014, doi: 10.1002/pi.4500.

[10] H. Mahfuz *et al.*, "Reinforcement of nylon 6 with functionalized silica nanoparticles for enhanced tensile strength and modulus," *Nanotechnology*, vol. 19, no. 44, 2008, doi: 10.1088/0957-4484/19/44/445702.

[11] O. Faruk, A. K. Bledzki, H. P. Fink, and M. Sain, "Biocomposites reinforced with natural fibers: 2000-2010," *Prog. Polym. Sci.*, vol. 37, no. 11, pp. 1552–1596, 2012, doi: 10.1016/j.progpolymsci.2012.04.003.

[12] S. Sinha-Ray *et al.*, "Supersonic nanoblowing: A new ultra-stiff phase of nylon 6 in 20-50 nm confinement," *J. Mater. Chem. C*, vol. 1, no. 21, pp. 3491–3498, 2013, doi: 10.1039/c3tc30248b.

[13] Z. Yang, W. Takarada, and H. Matsumoto, "Effect of the Fiber Diameter of Polyamide 11 Nanofibers on Their Internal Molecular Orientation and Properties.," *Macromol. Rapid Commun.*, vol. 44, no. 18, p. e2300212, Sep. 2023, doi: 10.1002/marc.202300212.

[14] M. V. Kakade, S. Givens, K. Gardner, K. H. Lee, D. B. Chase, and J. F. Rabolt, "Electric field induced orientation of polymer chains in macroscopically aligned electrospun polymer nanofibers," *J. Am. Chem. Soc.*, vol. 129, no. 10, pp. 2777–2782, 2007, doi: 10.1021/ja065043f.

[15] H. M. Heuvel, R. Huisman, and K. C. J. B. Lind, "Quantitative Information From X-Ray Diffraction of Nylon-6 Yarns - 1. Development of a Model for the Analytical Description of Equatorial X-Ray Profiles.," *J Polym Sci Part A-2 Polym Phys*, vol. 14, no. 5, pp. 921–940, 1976.

[16] S. S. Nair, C. Ramesh, and K. Tashiro, "Crystalline phases in nylon-11: Studies using HTWAXS and HTFTIR," *Macromolecules*, vol. 39, no. 8, pp. 2841–2848, 2006, doi: 10.1021/ma052597e.

[17] P. Čapková *et al.*, "Phase composition and surface properties of nylon-6 nanofibers prepared by nanospider technology at various electrode distances," *J. Polym. Res.*, vol. 22, no. 6, 2015, doi: 10.1007/s10965-015-0741-3.

[18] T. M. Ting, M. M. Nasef, and K. Hashim, "Tuning N-methyl-d-glucamine density in a new radiation grafted poly(vinyl benzyl chloride)/nylon-6 fibrous boron-selective adsorbent using the response surface method," *RSC Adv.*, vol. 5, no. 47, pp. 37869–37880, 2015, doi: 10.1039/c5ra00427f.

[19] M. M. Hall, V. G. Veeraraghavan, H. Rubin, and P. G. Winchell, "The approximation of symmetric X-ray peaks by Pearson type VII distributions," *J. Appl. Crystallogr.*, vol. 10, no. 1, pp. 66–68, 1977, doi: 10.1107/s0021889877012849.

[20] S. M. Aharoni, *n-Nylons : their synthesis, structure, and properties*. Chichester : Wiley, 1997. [Online]. Available: http://lib.ugent.be/catalog/rug01:000394343

[21] J. C. Ho and K. H. Wei, "Induced $\gamma \rightarrow \alpha$ crystal transformation in blends of polyamide 6 and liquid crystalline copolyester," *Macromolecules*, vol. 33, no. 14, pp. 5181–5186, 2000, doi: 10.1021/ma991702f.

[22] J. M. Schultz, B. S. Hsiao, and J. M. Samon, "Structural development during the early stages of polymer melt spinning by in-situ synchrotron X-ray techniques," *Polymer (Guildf).*, vol. 41, no. 25, pp. 8887–8895, 2000, doi: 10.1016/S0032-3861(00)00232-9.

[23] C. Ramesh and E. Bhoje Gowd, "High-temperature X-ray diffraction studies on the crystalline transitions in the α- and γ-forms of nylon-6," *Macromolecules*, vol. 34, no. 10, pp. 3308–3313, 2001, doi: 10.1021/ma0006979.

[24] Z. Zhao, W. Zheng, H. Tian, W. Yu, D. Han, and B. Li, "Crystallization behaviors of secondarily quenched Nylon 6," *Mater. Lett.*, vol. 61, no. 3, pp. 925–928, 2007, doi: 10.1016/j.matlet.2006.06.014.

[25] J. Ge *et al.*, "[Investigation of thermal behaviors of γ-form nylon 6 prepared by ammonia vapor from phosphoric acid solutions].,"

Guang Pu Xue Yu Guang Pu Fen Xi, vol. 32, no. 1, pp. 118–122, Jan. 2012.

[26] C. Feng, K. C. Khulbe, T. Matsuura, S. Tabe, and A. F. Ismail, "Preparation and characterization of electro-spun nanofiber membranes and their possible applications in water treatment," *Sep. Purif. Technol.*, vol. 102, pp. 118–135, 2013, doi: 10.1016/j.seppur.2012.09.037.

[27] J. Xue, T. Wu, Y. Dai, and Y. Xia, "Electrospinning and electrospun nanofibers: Methods, materials, and applications," *Chem. Rev.*, vol. 119, no. 8, pp. 5298–5415, 2019, doi: 10.1021/acs.chemrev.8b00593.

[28] C. V. Pious and S. Thomas, "Polymeric Materials-Structure, Properties, and Applications," *Print. Polym. Fundam. Appl.*, pp. 21–39, 2015, doi: 10.1016/B978-0-323-37468-2.00002-6.

[29] C. O. Mosiori, "Combustion synthesis and characterization of dysprosium nano-composite melilite," *Memories - Mater. Devices, Circuits Syst.*, vol. 4, no. March, p. 100042, 2023, doi: 10.1016/j.memori.2023.100042.

[30] D. Marlina, H. Hoshina, Y. Ozaki, and H. Sato, "Crystallization and crystalline dynamics of poly(3-hydroxybutyrate) / poly(4-vinylphenol) polymer blends studied by low-frequency vibrational spectroscopy," *Polymer (Guildf).*, vol. 181, no. August, p. 121790, 2019, doi: 10.1016/j.polymer.2019.121790.

[31] Z. Püspöki, M. Storath, D. Sage, and M. Unser, "Transforms and operators for directional bioimage analysis: A survey," *Adv. Anat. Embryol. Cell Biol.*, vol. 219, pp. 69–93, 2016, doi: 10.1007/978-3-319-28549-8_3.

[32] I. Lasenko, D. Grauda, D. Butkauskas, J. V. Sanchaniya, A. Viluma-Gudmona, and V. Lusis, "Testing the Physical and Mechanical Properties of Polyacrylonitrile Nanofibers Reinforced with Succinite and Silicon Dioxide Nanoparticles," *Textiles*, vol. 2, no. 1, pp. 162–173, 2022, doi: 10.3390/textiles2010009.

[33] A. Viluma-Gudmona, I. Lasenko, J. V. Sanchaniya, and B. Abdelhadi, "The amber nano fibers development prospects to expand the capabilites of textile 3D printing in the general process of fabrication methods," *Eng. Rural Dev.*, vol. 20, pp. 248–257, 2021, doi: 10.22616/ERDev.2021.20.TF051.

[34] D. Grauda, L. Bumbure, I. Lyashenko, A. Katashev, Y. Dekhtyar, and I. Rashal, "Amber particles as living plant cell markers in flow cytometry," *Proc. Latv. Acad. Sci. Sect. B Nat. Exact, Appl. Sci.*, vol. 69, no. 3, pp. 77–81, 2015, doi: 10.1515/prolas-2015-0011.

[35] A. Viluma-Gudmona, I. Lasenko, J. V. Sanchaniya, and A. Podgornovs, "Electro-resistant biotextile development based on fiber reinforcement with nano particles," *Eng. Rural Dev.*, vol. 20, pp. 804–812, 2021, doi: 10.22616/ERDev.2021.20.TF182.

[36] I. Lasenko *et al.*, "The Mechanical Properties of Nanocomposites Reinforced with PA6 Electrospun Nanofibers," *Polymers (Basel).*, vol. 15, no. 3, 2023, doi: 10.3390/polym15030673.

[37] V. Lusis *et al.*, "Experimental Study and Modelling on the Structural Response of Fiber Reinforced Concrete Beams," *Appl. Sci.*, vol. 12, no. 19, p. 9492, Sep. 2022, doi: 10.3390/app12199492.

[38] S. Gaidukovs, I. Lyashenko, J. Rombovska, and G. Gaidukova, "Application of amber filler for production of novel polyamide composite fiber," *Text. Res. J.*, vol. 86, no. 20, pp. 2127–2139, 2016, doi: 10.1177/0040517515621130.

[39] J. V. Sanchaniya, I. Lasenko, S. P. Kanukuntla, A. Mannodi, A. Viluma-Gudmona, and V. Gobins, "Preparation and Characterization of Non-Crimping Laminated Textile Composites Reinforced with Electrospun Nanofibers," *Nanomaterials*, vol. 13, no. 13, 2023, doi: 10.3390/nano13131949.

[40] J. V. Sanchaniya *et al.*, "Mechanical and Thermal Characterization of Annealed Oriented PAN Nanofibers," *Polymers (Basel).*, vol. 15, no. 15, 2023, doi: 10.3390/polym15153287.

[41] D. Grauda *et al.*, "Establishment of Biotesting System to Study Features of Innovative Multifunctional Biotextile," *Proc. Latv. Acad. Sci. Sect. B Nat. Exact, Appl. Sci.*, vol. 77, no. 3–4, pp. 186–192, 2023, doi: 10.2478/prolas-2023-0026.

[42] A. Hussain, V. Podgursky, D. Goljandin, M. Antonov, F. Sergejev, and I. Krasnou, "Circular Production, Designing, and Mechanical Testing of Polypropylene-Based Reinforced Composite Materials: Statistical Analysis for Potential Automotive and Nuclear Applications," *Polymers (Basel).*, vol. 15, no. 16, 2023, doi: 10.3390/polym15163410.

[43] A. Hussain, V. Podgursky, M. Viljus, and M. R. Awan, "The role of paradigms and technical strategies for implementation of the

circular economy in the polymer and composite recycling industries," *Adv. Ind. Eng. Polym. Res.*, vol. 6, no. 1, pp. 1–12, 2023, doi: 10.1016/j.aiepr.2022.10.001.

[44] A. Hussain, D. Goljandin, V. Podgursky, M. M. Abbas, and I. Krasnou, "Experimental mechanics analysis of recycled polypropylene-cotton composites for commercial applications," *Adv. Ind. Eng. Polym. Res.*, vol. 6, no. 3, pp. 226–238, 2023, doi: 10.1016/j.aiepr.2022.11.001.

[45] A. Asar and W. Zaki, "A comprehensive review of the mechanisms and structure of interpenetrating phase composites with emphasis on metal-metal and polymer-metal variants," *Compos. Part B*, vol. 275, no. October 2023, p. 111314, 2024, doi: 10.1016/j.compositesb.2024.111314.

[46] S. A. Kareem, J. U. Anaele, E. O. Aikulola, T. A. Adewole, M. O. Bodunrin, and K. K. Alaneme, "Design and selection of metal matrix composites reinforced with high entropy alloys – Functionality appraisal and applicability in service: A critical review," *J. Alloy. Metall. Syst.*, vol. 5, no. January, p. 100057, 2024, doi: 10.1016/j.jalmes.2024.100057.

[47] A. Shishkin, I. Hussainova, V. Kozlov, M. Lisnanskis, P. Leroy, and D. Lehmhus, "Metal-Coated Cenospheres Obtained via Magnetron Sputter Coating: A New Precursor for Syntactic Foams," *Jom*, vol. 70, no. 7, pp. 1319–1325, 2018, doi: 10.1007/s11837-018-2886-0.

[48] A. Shishkin *et al.*, "Cavitation-dispersion method for copper cementation from wastewater by iron powder," *Metals (Basel).*, vol. 8, no. 11, pp. 4–6, 2018, doi: 10.3390/met8110920.

[49] P. Colombo, "Cellular ceramics with hierarchical porosity from preceramic polymers," *IOP Conf. Ser. Mater. Sci. Eng.*, vol. 18, no. SPEC. SYMPOSIUM, 2011, doi: 10.1088/1757-899X/18/1/012002.

[50] V. Mironovs *et al.*, "Cellular structures from perforated metallic tape and its application for electromagnetic shielding solutions," *Agron. Res.*, vol. 12, p. (in Print), Jan. 2014.

[51] M. Pelanconi, D. Koch, G. Bianchi, S. Bottacin, and P. Colombo, "High-strength Si – SiC lattices prepared by powder bed fusion , infiltration-pyrolysis , and reactive silicon infiltration," no. December 2023, pp. 1–15, 2024, doi: 10.1111/jace.19750.